Architecture of the Protein-Conducting Channel Associated with the Translating 80S Ribosome

Roland Beckmann,[1,7,8] Christian M.T. Spahn,[2,3]
Narayanan Eswar,[4] Jürgen Helmers,[1]
Pawel A. Penczek,[5] Andrej Sali,[4] Joachim Frank,[2,3,6]
and Günter Blobel[1]
[1] Laboratory of Cell Biology
Howard Hughes Medical Institute
The Rockefeller University
1230 York Avenue
New York, New York 10021
[2] Howard Hughes Medical Institute, Health
    Research Inc.
[3] Wadsworth Center
Empire State Plaza
Albany, New York 12201
[4] Laboratory of Molecular Biophysics
Pels Family Center for Biochemistry
    and Structural Biology
The Rockefeller University
New York, New York 10021
[5] Department of Biochemistry
    and Molecular Biology
University of Texas–Houston Medical School
6431 Fannin
Houston, Texas 77030
[6] Department of Biomedical Science
State University of New York at Albany
Albany, New York 12222
[7] Institut für Biochemie der Charité
Humboldt Universität zu Berlin
Monbijoustr. 2,
10117 Berlin
Germany

Summary

In vitro assembled yeast ribosome-nascent chain complexes (RNCs) containing a signal sequence in the nascent chain were immunopurified and reconstituted with the purified protein-conducting channel (PCC) of yeast endoplasmic reticulum, the Sec61 complex. A cryo-EM reconstruction of the RNC-Sec61 complex at 15.4 Å resolution shows a tRNA in the P site. Distinct rRNA elements and proteins of the large ribosomal subunit form four connections with the PCC across a gap of about 10–20 Å. Binding of the PCC influences the position of the highly dynamic rRNA expansion segment 27. The RNC-bound Sec61 complex has a compact appearance and was estimated to be a trimer. We propose a binary model of cotranslational translocation entailing only two basic functional states of the translating ribosome-channel complex.

Introduction

A large number of mRNAs code for secretory and membrane proteins, which are translocated across, or inserted into, the membrane of the eukaryotic endoplasmic reticulum (ER) or the bacterial plasma membrane. In the case of cotranslational protein translocation, the translating ribosome is targeted in a signal sequence-dependent manner to the membrane, and associates with the protein-conducting channel (PCC) (Matlack et al., 1998). The so-called translocon is formed by association of the PCC with additional membrane protein complexes, which interact with the translocating polypeptide, such as the signal peptidase complex (SPC) and the oligosaccharyl transferase (OST) (Johnson and van Waes, 1999).

The PCC can specifically bind and insert a signal sequence, which leads to a high salt-resistant interaction with the ribosome (Görlich and Rapoport, 1993; Jungnickel and Rapoport, 1995; Kalies et al., 1994; Mothes et al., 1998) and to accessibility of an aqueous environment for the translocating peptide in the channel (Crowley et al., 1994; Gilmore and Blobel, 1985; Simon and Blobel, 1991). Hydrophobic domains of translocating nascent polypeptides have access to the hydrophobic core of the lipid bilayer and can partition from the channel into the membrane by lateral opening of the PCC (Borel and Simon, 1996; Heinrich et al., 2000; Martoglio et al., 1995). The cytosolic domains of membrane proteins are translated and released from the ribosome-channel complex (Mothes et al., 1997). The structural basis of these different activities of the PCC is unknown.

Importantly, during the different phases of polypeptide translocation or insertion, the ion permeability barrier of the membrane must be maintained. Based on fluorescence quenching studies using probes in the translocating nascent chain, it is believed that the necessary seal is provided by a tight junction between the translocon and the ribosome (Crowley et al., 1994). A diameter of 15 Å has been estimated for the aqueous pore in the inactive channel (plugged on the lumenal side by a Hsp70-like protein called BiP) by quenching experiments (Hamman et al., 1998), and of up to 60 Å for the pore of the active channel (Hamman et al., 1997). This creates a continuous space from the ER lumen through the channel into the tunnel of the large ribosomal subunit. For the release of cytosolic loops or transmembrane domains of nascent integral membrane proteins, the seal between ribosome and channel must be opened, which would lead to ion conductance. However, communication between the ribosome and the PCC has been suggested to coordinate the release of cytosolic loops with vertical and lateral gating of the channel such that an ion barrier is maintained at all times (Liao et al., 1997).

The PCC is formed in eukaryotic cells by the trimeric Sec61 complex, consisting of the Sec61α, β, and γ subunits (Sec61p, Sbh1p, and Sss1p in yeast) with, altogether, 12 transmembrane helices (Görlich and Rapoport, 1993; Wilkinson et al., 1996). Two-dimensional (2D) electron microscopy (EM) maps revealed that three to four Sec61 complexes could form ring-like structures of 100 Å diameter, with a central indentation or pore (Hanein et al., 1996). Similar oligomeric structures are

[8] Correspondence: roland.beckmann@charite.de

formed by the bacterial homolog, the SecYEG complex (Manting et al., 2000; Meyer et al., 1999). The first cryo-EM three-dimensional (3D) structure of the ribosome-Sec61 complex showed a donut-shaped Sec61 complex associated with the large ribosomal subunit (Beckmann et al., 1997). The channel is positioned such that its central pore is aligned with the exit of the tunnel in the large ribosomal subunit representing the conduit for the nascent chain. Surprisingly, a gap between the channel and the ribosome was observed, but it was attributed to the absence of a signal sequence, which was assumed to induce a tight seal formation (Beckmann et al., 1997). A recent cryo-EM study of mammalian ribosome-Sec61 complexes reported a similar spatial arrangement, with several connections forming the ribosome-channel junction, but still leaving a gap (Ménétret et al., 2000). This gap was observed with both purified Sec61 complexes and with less defined native translocons, and even under conditions where a signal sequence was assumed present. This led to a challenge of the current view of seal formation between ribosome and channel. It is difficult to understand, however, that these maps of presumably translating ribosomes show no tRNA density and that no conformational difference between active and inactive channels could be detected (Ménétret et al., 2000).

Taken together, it is not clear on what structural basis the ribosome-PCC complex can fulfill its different functions in cotranslational translocation without compromising the ion permeability barrier of the membrane. Here, we present a cryo-EM reconstruction of a complex containing the translating yeast 80S ribosome, a peptidyl-tRNA, a nascent polypeptide chain including a signal sequence, and the Sec61 complex at a resolution of 15.4 Å. The fact that the tRNA is visible with high occupancy gives us confidence that the complex indeed represents a translating ribosome. Based on homology modeling, we provide a molecular analysis of the complex and propose a mechanistic model for cotranslational translocation.

Results and Discussion

Programming, Purification, and Reconstitution of RNC-Channel Complexes

We chose a strategy to first isolate a homogenous population of ribosome-nascent chain complexes (RNCs) carrying a signal sequence, and then, in a second step, to use these RNCs for reconstitution of the RNC-channel complex in a membrane-free system for cryo-EM and 3D reconstruction. As a nascent chain, we used the first 120 amino acids of the yeast vacuolar type II membrane protein dipeptidylaminopeptidase B (DAP2), which is translocated cotranslationally in vivo (Ng et al., 1996). The transmembrane domain of this protein in positions 30 to 45 serves as an uncleaved signal sequence, which inserts into the membrane in a loop, resulting in a cytosolic orientation of the N terminus.

The ribosomes were programmed in a yeast cell-free translation system with a truncated synthetic mRNA lacking a stop codon. Under optimized conditions, this construct yielded 15%–20% stalled ribosome-nascent chain complexes, with the nascent chains still bound to

tRNA in the P site of the ribosome (data not shown). To immunopurify RNCs based on the presence of the nascent chain, we translated mRNA encoding for the 120 N-terminal residues with an additional N-terminal HA-tag (9 amino acids). Translation of the truncated mRNA of both the tagged and the untagged construct (called HA-DP120 and DP120) resulted in the appearance of two major bands on the autoradiography after SDS-PAGE (Figure 1a). The lower band represented the translated polypeptide; the larger product, migrating at about 40 kDa, represented the polypeptide still bound to tRNA (peptidyl-tRNA). A smear reaching from the higher to the lower band is a result of ongoing hydrolysis of the peptidyl-tRNA bond in the basic environment of the gel during the run (Figure 1a). Treatment with puromycin after translation led to a single band below 25 kDa and disappearance of the smear (data not shown). The translation products of the HA-tagged construct ran slightly higher than the untagged ones and were recognized by a monospecific antibody (Figure 1a, lower panel).

A crude ribosome fraction was isolated by spinning the translation reaction through a high salt/high sucrose cushion, which also resulted in dissociation of nonribosomal proteins from RNCs. The mixture of empty ribosomes and RNCs was then incubated with a biotinylated anti-HA antibody and streptavidin-coupled magnetic beads. After washing the beads with high salt and detergent containing buffers, the bound RNCs were eluted by incubation with an excess of corresponding HA-peptide and spun through a sucrose cushion again. For the tagged construct, this procedure resulted in a highly enriched RNC fraction (Figure 1b) with small amounts of detectable ribosomal proteins but a strong ^{35}S-signal due to the presence of labeled nascent chains. Most importantly, however, the purification procedure did not lead to any detectable background when performed with the untagged control construct (DP120, Figure 1b). We scaled up the procedure to purify sufficiently large amounts (0.25 OD$_{260}$, $\sim$5 pmol) for further studies. The isolated RNCs showed the characteristic pattern of ribosomal proteins (Figure 1c) and were stable for at least 9 hr on ice without significant hydrolysis or dissociation of the peptidyl-tRNA (data not shown). Thus, we describe a method for the isolation of a homogenous fraction of programmed (80S) ribosomes, which (1) carry a chosen nascent chain kept in place by the P site tRNA, (2) are virtually free of empty ribosomes and additional factors, (3) are stable enough for further experiments, and (4) can be isolated in quantities sufficient for biochemical and structural studies.

Next, we attempted to reconstitute the active, i.e., translating and translocating, ribosome-channel complex using the RNC preparation and purified Sec61 complex in a membrane-free system. The length of the nascent chain (HA-DP120) was chosen such that the signal sequence and at least 40 additional amino acids between the signal sequence and the C terminus should be fully emerged from the tunnel of the large ribosomal subunit (Blobel and Sabatini, 1970). This configuration is known to facilitate a productive interaction of the signal sequence, with the channel leading to the insertion of the nascent chain as a loop (Jungnickel and Rapoport, 1995; Mothes et al., 1998; Shaw et al., 1988).
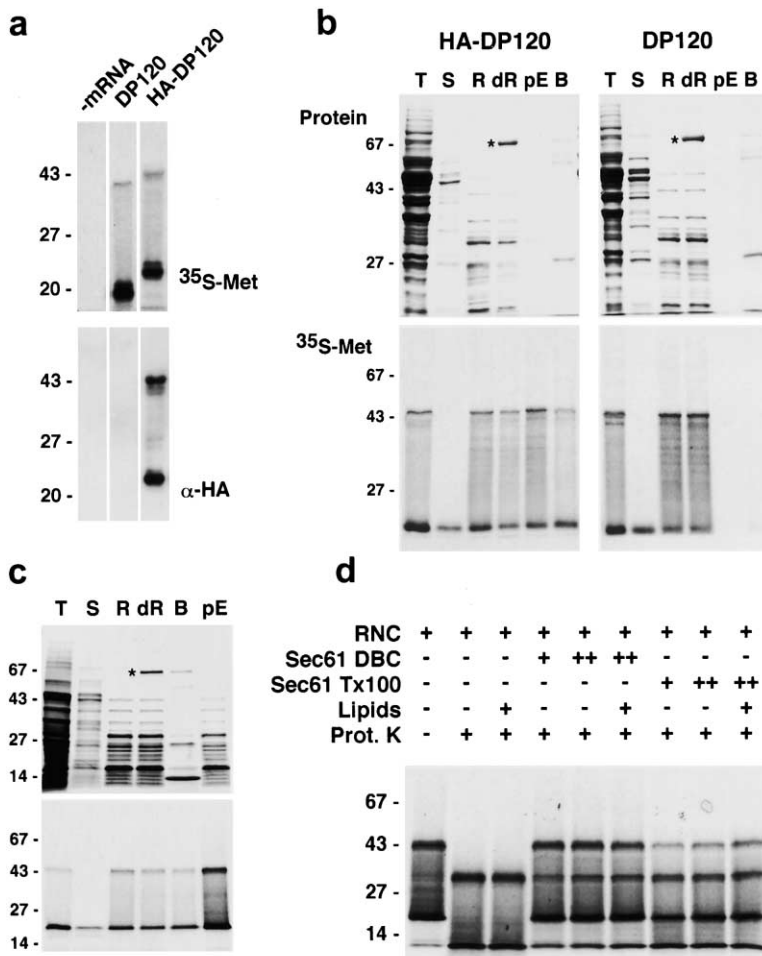
a

43 -
27 -
20 -

35S-Met

43 -
27 -
20 -

α-HA

b

HA-DP120   **DP120**

T S R dR pE B   T S R dR pE B

Protein

67 -
43 -
27 -

35S-Met

67 -
43 -
27 -

c

T S R dR B pE

67 -
43 -
27 -
14 -

67 -
43 -
27 -
14 -

1/50   1   1/10

d

RNC	+	+	+	+	+	+	+	+	+
Sec61 DBC	-	-	-	+	++	++	-	-	-
Sec61 Tx100	-	-	-	-	-	-	+	++	++
Lipids	-	-	+	-	-	+	-	-	+
Prot. K	-	+	+	+	+	+	+	+	+

67 -
43 -
27 -
14 -

Figure 1. Immunopurification of RNCs and Reconstitution of the RNC-Sec61 Complex

(a) Truncated mRNA coding for the first 120 amino acids of dipeptidylpeptidase B with (HA-DP120) or without (DP120) N-terminal HA-tag was translated in a yeast cell-free system in the presence of ^{35}S-labeled methionine. The translation reaction was subjected to SDS-PAGE, blotted onto nitrocellulose, and either autoradiographed (top) or probed using a monoclonal anti-HA antibody (bottom).

(b) Translation reactions with tagged and untagged nascent chains were subjected to an analytical immunopurification procedure. Aliquots of fractions were applied to SDS-PAGE, blotted onto nitrocellulose, amido black stained (Protein), and autoradiographed to detect nascent polypeptide chains (^{35}S-Met). T, total; S, supernatant; R, crude ribosomes; dR, depleted crude ribosomes after antibody and magnetic bead incubation; pE, eluate using excess HA-peptide; B, magnetic beads after elution. Note the enrichment of HA-DP120 RNCs (pE) and the background-free control eluate (pE for DP120). Asterisks mark bovine serum albumin, which is part of the antibody preparation.

(c) Same as shown for HA-DP120 in (b) but upscaled for preparative purpose. Note the characteristic pattern of ribosomal proteins in the peptide eluate (pE).

(d) Immunopurified RNCs carrying the HA-DP120 chain were reconstituted with different amounts of solubilized Sec61 complex in DeoxyBigChap (DBC) or Triton X-100 detergent in the presence or absence of phospholipids. Subsequently, the samples were subjected to protease digestion by incubation with proteinase K and analyzed by SDS-PAGE followed by autoradiography.

The RNCs were incubated with increasing amounts of solubilized Sec61 complex under different conditions and, subsequently, nascent chain insertion was monitored by protease protection assays. After digestion with proteinase K of RNCs alone, the nascent chain signal shifted completely to a lower molecular weight (regardless of the presence or absence of lipids), demonstrating that only a small part, buried in the ribosomal tunnel (30–35 aa), was protected (Figure 1d). However, incubation of the RNCs with the Sec61 complex resulted in protection of the full-length chain with different degrees of efficiency; most efficient was an excess of Sec61 complex in the detergent DeoxyBigChap (DBC), leading to a fraction of approximately 75%–85% protected chains. Higher concentrations of the Sec61 complex or the presence of phospholipids did not significantly change the degree of protection. In contrast, incubation with the Sec61 complex in Triton X-100 led only to 15%–25% protected chains (Figure 1d). Thus, by using RNCs with the solubilized Sec61 complex in DeoxyBigChap, we successfully reconstituted an active RNC-channel complex with fully inserted nascent chain. This result agrees well with the results of previous experiments demonstrating (1) that the channel interacts with the ribosome in detergent solution (Beckmann et al., 1997; Prinz et al., 2000), (2) that direct and productive

interaction of RNCs with the channel can take place without involvement of the SRP/SR targeting system (Jungnickel and Rapoport, 1995), and (3) that the mammalian Sec61 complex, as well as the heptameric Sec complex from yeast, display translocation activity in detergent solution (Matlack et al., 1997; Mothes et al., 1998).

Reconstruction and Overall Structure of the RNC-Channel Complex

The RNC-channel complex reconstituted in DBC was used for structure determination by cryo-EM and single particle reconstruction. As a control, empty ribosomes were isolated from a translation system lacking mRNA and reconstituted under the same conditions with the Sec61 complex. Figure 2 shows the structures of the active and inactive complexes determined at a resolution of 15.4 Å and 18.9 Å, respectively, based on the Fourier shell correlation criterion using a cutoff at 0.5 (corresponding to 10.9 Å and 13.7 Å using a cutoff at 3σ). The lower resolution of the nontranslating ribosome is most likely a result of higher conformational variability, due to a less defined functional state of the ribosome. The 15.4 Å (10.9 Å) reconstruction represents the highest resolution achieved so far for an eukaryotic 80S ribosome. It was further processed to separate rRNA from
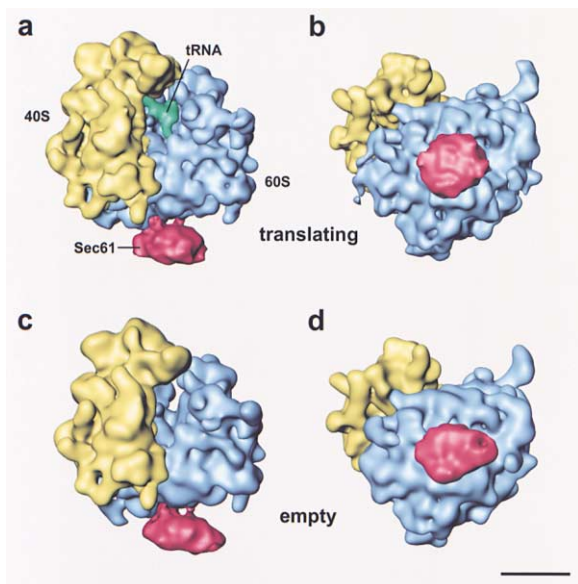
Figure 2. Cryo-EM Structures of the Translating and the Empty Ribosome-Sec61 Complex

(a) Reconstruction of the translating and translocating RNC-Sec61 complex in DBC at 15.4 Å resolution. Note the presence of tRNA density in the P site and the Sec 61 channel with the shape of a compact disk in the active complex. Color coding: yellow, small ribosomal subunit (40S); blue, large ribosomal subunit (60S); red, Sec61 complex; green, P site tRNA.
(b) Same as (a) but rotated upward by 90°.
(c) Reconstruction of the empty complex in DBC at 18.9 Å resolution. Note the absence of tRNA density and the elongated shape of the channel. Color coding as described for (a).
(d) Same as (c) but rotated upward by 90°. Bar = 100 Å.

protein densities (Spahn et al., 2000) and interpreted by docking of rRNA and protein structure models (see accompanying paper by Spahn et al., 2001 [this issue of *Cell*]).

Both structures show the same overall appearance typical for the yeast 80S ribosome, with the small (40S) and large (60S) ribosomal subunits clearly recognizable (Figure 2) (Beckmann et al., 1997; Gomez-Lorenzo et al., 2000; Morgan et al., 2000). Extra density, representing the Sec61 complex, is visible in both reconstructions at the exit site of the large ribosomal subunit tunnel, which is believed to function as a conduit for the nascent chain (Beckmann et al., 1997; Bernabeu et al., 1983; Nissen et al., 2000). The shape of the PCC in its active and inactive state is similar to the shape we observed before (Beckmann et al., 1997), with a gap of at least 15 Å between the channel surface and the ribosome, regardless of the presence of a signal sequence. However, in both states, additional connections between the PCC and the ribosome are visible and, interestingly, the PCC now appears as a compact disk with a central indentation rather than a toroidal mass with a central pore. The inactive PCC is somewhat flattened in the direction perpendicular to the plane of the membrane and elongated in the plane of the membrane when compared to the active PCC. Furthermore, additional density is visible in the intersubunit space of the programmed ribosome, unambiguously recognizable as tRNA.

To quantify the occupancy of RNCs with channel and to obtain additional confirmation of the contour levels chosen in this study, we sorted the translating complex particles computationally, dependent on the presence of density in the channel region (C.M.T.S., P.A.P., J.F., unpublished data). The particle distribution between the two resulting populations indicated that about two-thirds of the ribosomes were carrying the channel, which agrees approximately with the degree of nascent chain protection in the protease protection assay (Figure 1d). The reconstruction of the two subsets yielded two structures, both with clearly visible tRNA densities. As expected, only one of the structures had a channel density. The shape of this density is essentially identical to the structure shown, but the relative density of the channel is stronger (data not shown).

Presence of tRNA in the Programmed Ribosome
The tRNA density is shown with the same contour level as the ribosome. It is located in the P site of the ribosome and corresponds to an occupancy of at least 80%–90% of the ribosomes (Figure 2; see also Spahn et al., 2001). Difference maps, using programmed and empty ribosomes, did not reveal any significant occupancy of the A site or E site with tRNA. tRNAs occupying A or E site were probably removed during the wash step using high salt concentrations. This result demonstrates that the translation of truncated mRNA indeed leads to a stalled peptidyl-tRNA, with the vast majority tightly bound to the P site in a manner resistant to high salt concentrations. Furthermore, these results confirm the efficiency of the new protocol and the quality of the resulting preparation. The high occupancy of ribosomes with peptidyl-tRNA serves as proof for the presence of the signal sequence-containing nascent chain, which is small ($\sim$14 kDa) and too elongated to be visualized at this resolution. Similarly, cryo-EM visualization of 70S ribosomes charged with tRNA in vitro (Agrawal et al., 1996, 2000) or of translating dimeric ribosomes formed in vivo (Stark et al., 1997) also led to clearly identifiable tRNA densities in the intersubunit space. Therefore, the presence of the tRNA density in our map served as a prerequisite to permit the interpretation of the structures based on different functional states.

Movement of the Expansion Segment 27
Close to the channel attachment site, the large subunit bears a rod-like density 150 Å in length with a twist typical for helical rRNA. The density originates at the subunit interface and was identified as the main helix of expansion segment 27 (ES27) of 25S rRNA (Spahn et al., 2001), one of the rRNA insertions characteristic for 80S ribosomes (Gerbi, 1996). In several reconstructions of different nontranslating yeast ribosome complexes (Beckmann et al., 1997; Gomez-Lorenzo et al., 2000; Morgan et al., 2000; and not shown), this helix can be found close to the L1 arm ("L1 position"), but also, following a counterclockwise rotation by 90°, reaching over the tunnel exit site ("exit position"). A distance of approximately 15 Å between the tip of the helix and the tunnel exit leaves sufficient space for the nascent chain to emerge from the ribosome. The preference for one or the other position varies in these reconstructions, and
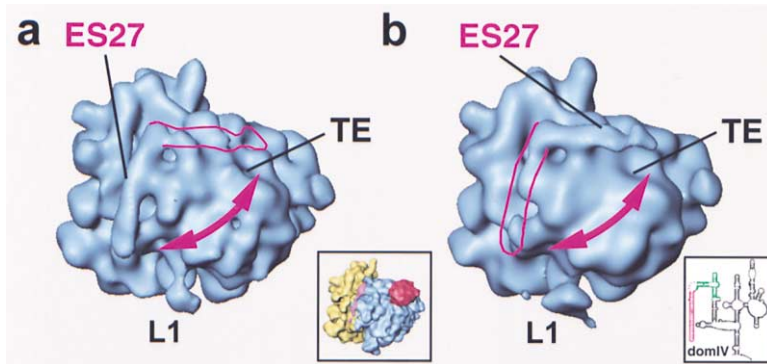
Figure 3. Dynamic Expansion Segment 27 (ES27)

(a) The reconstruction of a ribosome-Sec61 complex in Triton X-100 (Beckmann et al., 1997) shown without the channel density. TE marks the tunnel exit and L1 the L1 protrusion. Note the expansion segment 27 (ES27) in the L1 position, distant from the tunnel exit. The pink contour shows the exit position of ES27 as observed in (b). Left inset: the 15.4 Å reconstruction in the same orientation as the maps in (a) and (b) with the color code used in Figure 2 and ES27 in the L1 position colored pink. Right inset: Secondary structure diagram of domain IV of *S. cerevisiae* 25S rRNA with colored ES27 (green and pink) and the moving helix labeled pink (diagram from R.R. Gutell, http://www.rna.icmb.utexas.edu).

(b) A reconstruction of the ribosome without attached Sec61 complex at a resolution of 24.8 Å. Note that in this structure no density is visible in the L1 position. Instead, the ES27 is in the exit position with its tip in close proximity to the tunnel exit. The pink contour shows the L1 position as observed in (a).

the density is often present in both positions. Therefore, the ES27 helix is a highly dynamic structure with two main conformations in functional equilibrium (Figure 3). Notably, in reconstructions of ribosome-channel complexes, the ES27 helix was located exclusively in the L1 position, thereby not interfering with the channel in the exit position (Figure 3). Thus, binding of the channel to the ribosome must coincide with a conformational change in the ribosomal periphery, shifting the equilibrium for the ES27 helix entirely to the L1 position.

We suggest that this rotating rRNA structure may play a role in coordinating access of nonribosomal factors, such as chaperones, modifying enzymes, SRP, or the translocon to the tunnel exit site and thereby to the emerging nascent chain. In addition, the segment may interact directly with the nascent chain or with nascent chain-interacting proteins. In any case, the function of ES27 is essential and conserved. It has been demonstrated in *Tetrahymena* that deletion of this insertion is lethal but can be complemented with a corresponding insert from other species (Sweeney et al., 1994). After the L1 protuberance (Gomez-Lorenzo et al., 2000), the ES27 helix is the second example of an extremely dynamic rRNA segment in the periphery of the 80S ribosome.
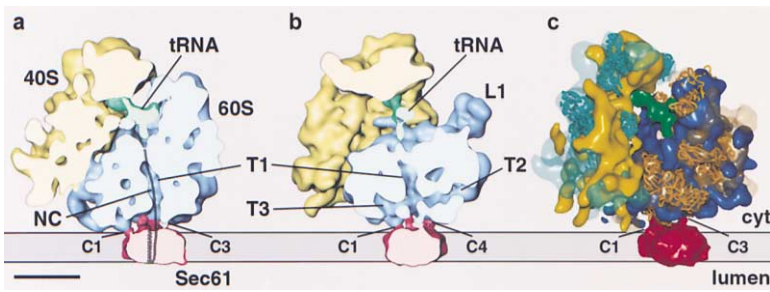
The Ribosome-Channel Connection
The connection between ribosome and channel is not circumferentially sealed, but leaves a lateral opening of ~15 Å (Figures 2, 4, and 5) in both reconstructions. This finding is similar to what has been observed at lower resolution in several ribosome-channel reconstructions from yeast as well as from mammalian complexes (Beckmann et al., 1997; Ménétret et al., 2000). There are no significant differences in the dimensions of these gaps when comparing active and inactive complexes (Figures 2 and 4). Even at very low contour levels, the ribosome-channel connection is never completely sealed regardless of the functional state (not shown). This observation agrees well with protease protection experiments showing that emerging nascent chains are accessible to added protease when they are either too short to interact productively with the channel or form extended cytosolic loops (Hegde and Lingappa, 1996;

Jungnickel and Rapoport, 1995). It also agrees with the finding that nascent chains such as preprolactin 86mer and the substrate used in this study are protected from digestion. These nascent chains form a loop reaching directly from the tunnel exit into the channel, with the space between the channel surface and ribosome being too small for the protease to enter (Jungnickel and Rapoport, 1995; Shaw et al., 1988).

However, with a lateral opening as large as 15 Å, it is unlikely that the ribosome-channel connection can function as an ion-tight seal maintaining the ion permeability barrier of the ER membrane, as suggested based on fluorescence quenching experiments (Crowley et al., 1994; Hamman et al., 1997). It is possible, however, that it is not the PCC itself, but lipids or additional proteins that lead to the observed seal formation in native mammalian membranes. On the other hand, a seal formed by the ribosome-membrane junction may be ineffective in light of the existence of additional tunnels in the large ribosomal subunit (T2 and T3, Figure 4), which are also present in bacterial and archaebacterial ribosomes (Ban et al., 2000; Frank et al., 1995; Gabashvili et al., 2001). Since these tunnels connect the conduit for the nascent chain with the cytosolic environment, they may allow ion flow between the cytosol and the ER lumen, even if a seal-forming junction between ribosome and membrane is present (Figure 4).

Docking of rRNA and protein models into separated rRNA and protein densities (see Spahn et al., 2001) allowed the analysis of the PCC attachment sites at the molecular level (Table 1). In both functional states, the channel is attached to the ribosome with the same connections, one of which we observed before (connection 1) at lower resolution (Beckmann et al., 1997). Connection 1 is formed by a protrusion consisting of the helix 59 of rRNA domain III and the N-terminal domain of the ribosomal protein rpL19 (Table 1). However, three additional connections are now visible (Figures 4 and 5). Connection 2 most likely also involves rRNA domain III (helix 53 and helix 50) and the N-terminal domain of rpL19 as well as rpL25. Connection 3 is in closest proximity to the tunnel exit engaging rRNA helix 24 of domain I and, in addition, an extended loop of rpL26. Connection 4 is the most substantial one, involving two

Figure 4. Connections, Gaps, and Tunnels in the RNC-Sec61 Structure

(a) The 15.4 Å reconstruction of the RNC-Sec61 complex as shown in Figure 2a but cut perpendicularly to the plane of the membrane along the tunnel in the large ribosomal subunit. Color code as in Figure 2. C1 to C4 mark the connections between the ribosome and the channel. T1 marks the vertical tunnel, which functions as conduit for the nascent chain. The expected path of the nascent chain is indicated (NC). Note the gap between the ribosome and the channel. Cyt, cytosolic side; lumen, ER lumen. Bar = 100 Å.

(b) As in (a) but rotated by 60° around the z axis. T2 and T3 indicate the position of two horizontal tunnels connecting the main vertical tunnel (T1) with the cytosolic environment. Note the gap between the ribosome and the channel.

(c) Structure of the RNC-Sec61 complex after separating rRNA and protein densities, and docking of homology protein structure models into their densities. Color code: red, Sec61 complex; green, P site tRNA; blue, 25S/5S rRNA density; transparent orange, 60S protein density; orange, backbone of 60S protein models; yellow, 18S rRNA density; transparent turquoise, 40S protein density; turquoise, backbone of 40S protein models. Note the gap between the ribosome and the channel, and the presence of rRNA as well as protein near the channel connections.

ribosomal proteins, rpL25 and rpL35, and the tip of rRNA helix 7 of domain I (Figures 4 and 5). It is interesting to find that ribosomal proteins are most likely involved in all ribosome-channel connections. The isolated rRNA of the large ribosomal subunit was shown to be sufficient to bind to the channel with high affinity, even across different species (Prinz et al., 2000). However, in contrast to other parts of the ribosomal periphery, the entire region near the tunnel exit, including rRNA as well as proteins, appears to be relatively conserved. At a resolution between 25–30 Å, the mammalian ribosome has also a very similar appearance in this region (Morgan et al., 2000), and four ribosome-channel connections have been observed in similar positions (Ménétret et al.,
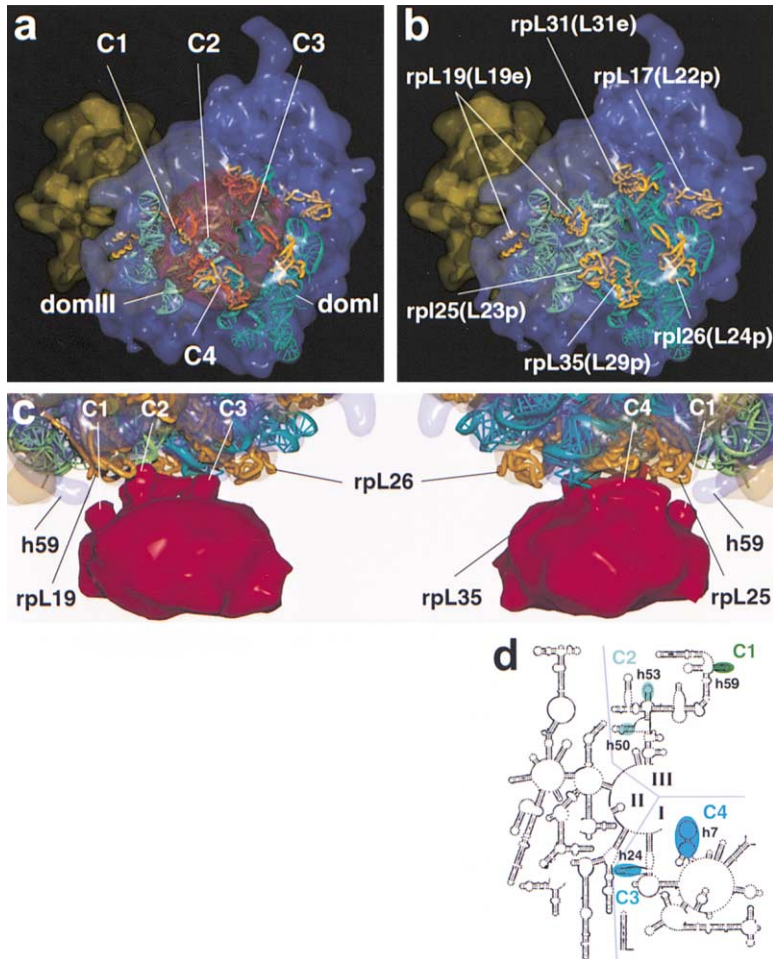

Figure 5. Molecular Analysis the RNC-Sec61 Connections

(a) The RNC-Sec61 complex is shown in the same orientation and color code as in Figure 2b with transparent densities. Docked models of the 25S rRNA domains (turquoise, domI; green, domIII) involved in channel attachment and the backbones of homology models (orange) of the ribosomal proteins near the tunnel exit are shown. The positions of the four connections (C1–C4) are indicated by holes in the Sec61 density. Note the particularly strong participation of ribosomal proteins in connection 4.

(b) Same as in (a) but without the Sec61 density. Proteins are labeled according to the yeast nomenclature with the corresponding ribosomal protein family name given in parenthesis.

(c) Close up of the RNC-Sec61 junction in a similar orientation as in Figure 2a (left side) and rotated 180° around the z axis (right side). The separated 25S rRNA and the 60S protein densities are shown in transparent blue and transparent orange, respectively. Docked models of the 25S rRNA domain I (turquoise), domain III (green), and proteins (orange) are shown as ribbons. The positions of the four connections (C1–C4) are indicated. Density for helix 59 of rRNA domain III is marked by h59. Participation in connection 1, rRNA domain III and rpL19 (L19e); connection 2, rRNA domain III and rpL19 (L19e); connection 3, rRNA domain I and rpL26 (L24p); connection 4, rRNA domain I, rpL25 (L23p) and rpL35 (L29p). For details see Table 1.

(d) Secondary structure diagram of the yeast 25S rRNA domains I, II, and III (diagram from R.R. Gutell, http://www.rna.icmb.utexas.edu). The regions involved in connection are labeled accordingly (for details see Table 1).

Table 1. Molecular Analysis of the Ribosome-Channel Connections

Connection	Protein	Position (yeast models)	25S rRNA	Position (archea model)
1	rpL19 (L19e)	P25–T48	helix 59 (domIII)	G1627–G1634
2	rpL19 (L19e)	P25–T48	helix 53 (domIII)	G1498–C1507
	rpL25 (L23p)	S68–I80	helix 50 (domIII)	C1421–A1424
3	rpL26 (L24p)	T86–P96	helix 24 (domI)	G504–G487
4	rpL25 (L23p)	S68–I80, A127–A135	helix 7 (domI)	G81–G94
	rpL35 (L29p)	A2–K5, K25–K49		

2000). This region is also similar comparing the yeast ribosome with the archeabacterial 50S subunit (Nissen et al., 2000), an important difference being a shorter rRNA helix 59 in *H. marismortui*. This helix in the bacterial *E. coli* ribosome (Gabashvili et al., 2000) is comparable in length to the yeast ribosome, but a rpL19-like protein is missing (L19e in *Archea*). Thus, despite the fact that there are some differences, the overall spatial arrangement of the ribosome-channel interaction is conserved in bacterial, archeabacterial, and eukaryotic cells and involves both large subunit RNA and proteins.

Structure and Function of the Protein-Conducting Channel

The dimensions of the PCC are similar to findings of earlier EM studies (Beckmann et al., 1997; Hanein et al., 1996; Ménétret et al., 2000). The distance between cytosolic and lumenal surface is approximately 48 Å, hence easily spanning the membrane. The diameter of the translocating channel is between 85 and 95 Å (Figure 6). The channel associated with the empty ribosome appears slightly flattened and elongated toward the back of the large ribosomal subunit with a diameter of approximately 100 Å. This elongation is lost at higher contour levels, where translocating and nontranslocating channels appear more similar (data not shown). Al-

though the shape of the channel displays structural details, the slightly pentagonal shape, which was described in previous studies of the Sec61 complex (Beckmann et al., 1997; Hanein et al., 1996) and in one study of its bacterial homolog, the SecYE complex (Meyer et al., 1999), is not recognizable.

For estimating the Sec61 oligomer stoichiometry, we used the shape of the channel in the following way: each Sec61 trimer is believed to have 12 membrane-spanning helices plus two amphipathic helices (Johnson and van Waes, 1999; Wilkinson et al., 1996). Assuming membrane-specific helix packing, we determined the number of helices of known membrane protein structures that could fit into the channel density. This approach is reliable even in the presence of flexible and thereby invisible domains outside the membrane, in contrast to calculations based on observed volume and specific protein density. Assuming less dense packing in the central region, the outline of the channel offers space for 35 helices, for example provided by five rhodopsin molecules (Palczewski et al., 2000) (Figures 6b and 6c). This helix packing corresponds to an average area between 180 and 190 Å^2/helix, which is in good agreement with experimental data (184 Å^2/helix for rhodopsin and 186 Å^2/helix for bacteriorhodopsin; for review see Collinson et al., 2001). This result argues strongly in favor
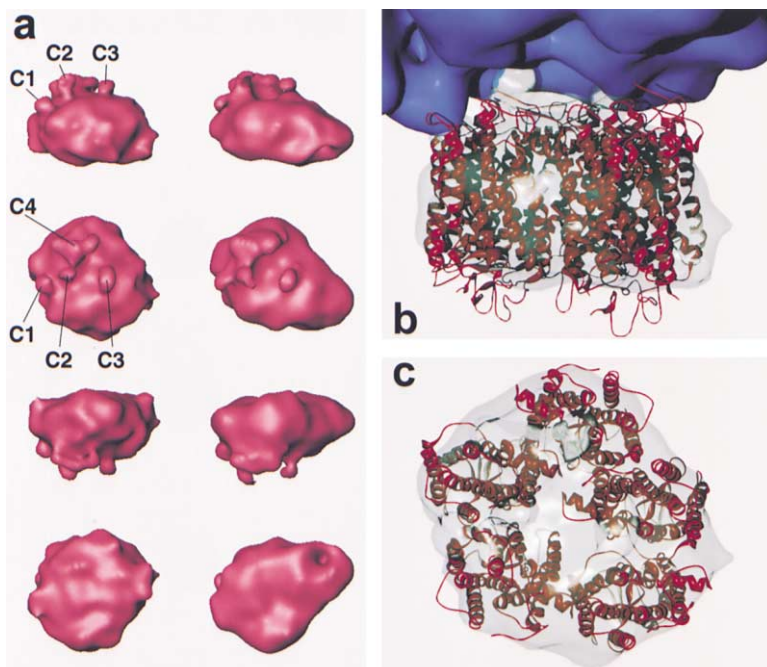

Figure 6. Structure and Stoichiometry of the Protein-Conducting Channel

(a) Isolated density of the Sec61 complex in the translocating state (left column) and the inactive state (right column). The view on top is the same as in Figures 2a and 2c. The views below are rotated 90°, 180°, and 270° toward the viewer. The four connections are marked by C1 through C4. Note the central indentation at the surface facing the ER lumen and the ribosome. The channel attached to the empty ribosome appears elongated and flattened compared to the one engaged in translocation.

(b) Closeup of the RNC-Sec61 junction in the same orientation as in (a), with the large ribosomal subunit shown in blue and the Sec61 complex in transparent green. In order to estimate the stoichiometry of the Sec61 oligomer, the transmembrane helices of five rhodopsin molecules (red ribbons) were fitted into the channel density.

(c) Top view of (b), but only the channel density with fitted membrane domains. The number of approximately 35 helices fitting into the density suggests a trimer of Sec61 trimers (36 helices).
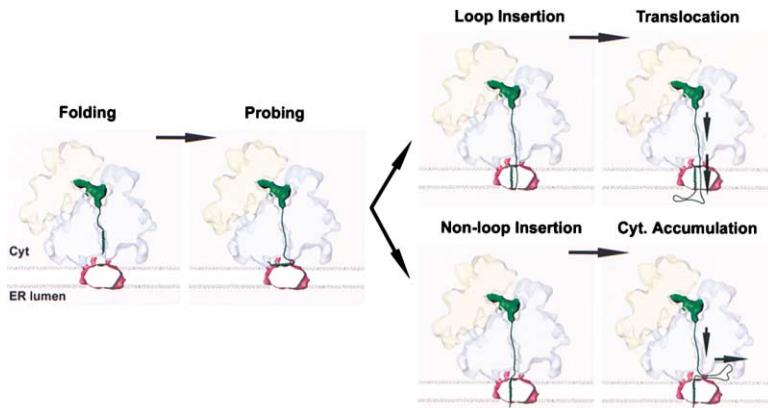
Figure 7. Binary Model of Cotranslational Protein Translocation

The model is based on the finding that a gap exists between the RNC and the PCC, and that the translating PCC has a compact conformation. Hence, the PCC can provide a seal to maintain the ion permeability barrier of the ER membrane:
(1) The tunnel in the large ribosomal subunit facilitates folding of α-helical segments.
(2) The emerging segment is probed by the PCC before insertion. Hydrophobicity, helicity, and the nature of the flanking regions (i.e., positive charges) determine if and in what orientation the segment is inserted.
(3) Insertion can occur in two different orientations with the channel opening just wide enough to accommodate the inserted na-

scent polypeptide.
(4) In case of *loop insertion*, the following nascent chain is guided through the membrane, and translocation is possible. In case of *non-loop insertion*, the following nascent chain cannot translocate, accumulating on the cytosolic side of the membrane. Because of the sealed channel and the existence of the gap between ribosome and PCC, such cytosolic domains can easily exit into the cytosol at any time without compromising the ion permeability barrier.
Nascent chain translocation after loop insertion and cytosolic accumulation after non-loop insertion are the only two principally different functional states of the RNC-PCC complex. A simple secretory protein would experience only one loop insertion of the signal sequence after targeting by SRP and translocate. For a polytopic membrane protein, the states would alternate with every new hydrophobic transmembrane domain. This model may be expanded by including additional regulation (i.e., pause transfer sequences [Chuck and Lingappa, 1992]) and exceptions.

of three Sec61 trimers forming the isolated active PCC. For the homologous SecYEG complex, it was reported that a slightly higher average area of 199 Å^2 per helix is occupied in the plane of the membrane (Collinson et al., 2001). If this area is similar for the Sec61 complex, the observed part of the density map could encompass approximately 33 transmembrane helices, still supporting the estimation of three Sec61 trimers per channel. The lack of a 3-fold rotational symmetry may be a feature of the channel itself, or could be induced by the asymmetric interaction with the ribosome.

Remarkably, in both functional states, the channel appears compact and has only a small indentation instead of a central pore (Figure 6). This indicates that the interaction with the signal sequence does not necessarily lead to a widely open channel conformation. It appears compact in both maps, even at higher contour levels, a result which is different from our previous observation with the empty ribosome-channel complex in Triton X-100 detergent solution (Beckmann et al., 1997). The open conformation in Triton X-100 may be induced by this strong detergent and may explain the accessibility of the nascent chain to protease under these conditions (Figure 1d). The slightly flattened and more elongated shape of the inactive channel could indicate that gating by the signal sequence leads to a small rotation of the membrane helices toward a position more perpendicular to the plane of the membrane. This iris-like movement would be reminiscent of the conformational change suggested for the gating of gap junctions (Unwin and Zampighi, 1980). Our results do not support conclusions from fluorescence quenching experiments with native mammalian ER membranes suggesting a pore of 9–15 Å diameter in the inactive translocon (Hamman et al., 1998), and of 40–60 Å diameter in the translocating one (Hamman et al., 1997). Yet, in contrast to the purified channels used by us, the channels in native membranes

are known to be associated with additional proteins in different oligomeric states (Ménétret et al., 2000; Wang and Dobberstein, 1999). In a recent cryo-EM study of mainly mammalian ribosome-channel and mixed ribosome-translocon complexes (Ménétret et al., 2000), the channels are shown with open conformations. However, the contour levels, chosen in that study based on a molecular weight/specific density calculation, appear to be very high. At slightly lower, more realistic contour levels, closed conformations of the channels are visible, which is in accord with our results. Taken together, in all studies of the eukaryotic PCC, using either 2D (Hanein et al., 1996) or 3D reconstructions (Beckmann et al., 1997; Ménétret et al., 2000), a central pore or at least an indentation has been observed, which is juxtaposed to the nascent chain tunnel exit of the ribosome. This result is a strong indication that the central region in the channel is less dense and very flexible, in accordance with its function in protein conductance across the membrane.

Binary Model of Cotranslational Translocation and Membrane Protein Insertion

We observed the translocating channel in a compact conformation, and a gap between the channel and the ribosome. The compact appearance indicates that gating of the channel by the signal sequence can lead to an opening just large enough to be completely occupied by the inserted nascent polypeptide chain (Figures 3 and 7) without allowing ion conductance. Based on these findings, we propose a binary model, describing how the ribosome-PCC complex could function in cotranslational translocation and membrane protein insertion (Figure 7). First, we suggest that the conserved tunnel in the large ribosomal subunit represents an important functional domain of the ribosome, allowing exclusively the folding of α-helical secondary structure. The tunnel

dimensions are such that α-helix folding is supported, but β sheet formation is sterically unlikely, because the average tunnel diameter of 15 Å is too small. A preferred sequence of folding events starting with α-helix formation would provide folding seeds along the sequence and considerably reduce the difficulty of folding. In the translocation context, it has been shown that helicity as well as hydrophobicity of a signal sequence are necessary for its productive interaction with the signal recognition particle (SRP) and with the PCC (Keenan et al., 2001; Plath et al., 1998). Probing of the nascent chain for hydrophobic helices by the channel would lead to the insertion and capture of any sufficiently hydrophobic segment in such a way that the inserted polypeptide is tightly accommodated. Depending upon its orientation in the channel, the hydrophobic segment can expose its C-terminal end either to the cytosolic or to the lumenal side, in the latter case resulting in loop formation of the remaining nascent chain in the channel (Figure 7). Importantly, insertion would not lead to further opening of the pore to any predefined size. As a result, the following nascent chain will either accumulate on the cytosolic side or, only if it has been coinserted in a loop, translocate across the membrane. This scenario would have two major implications: (1) After ribosome targeting to the PCC, further events are almost exclusively dependent on the presence and nature of hydrophobic segments and their interaction with the channel, especially their preferred orientation for channel insertion. (2) The channel itself would have the property of a seal, preventing ion flow across the membrane independent of the presence of the ribosome. It would require that the pore accessible to hydrated ions in the presence of a translocating chain is not larger than 6 Å in diameter (Johnson and van Waes, 1999). How could the channel provide such flexibility? One possibility is that the overall arrangement of transmembrane helices and subunits can be adjusted accordingly. At the same time, as observed for SRP (Keenan et al., 2001), flexible amino acid side chains could behave like bristles to provide the appropriate environment and accommodate the large number of different translocating polypeptide chains.

Conclusions

Using immunopurified RNCs for a molecular analysis of the RNC-PCC complex, we find conserved rRNA segments as well as proteins involved in forming the ribosome-channel junction. We observe the translocating channel in a compact conformation and a gap between the channel and the ribosome. This observation provides the basis for a binary model of cotranslational translocation. The model needs to postulate only two principally different functional states of the RNC-PCC complex to explain the translocation of secretory proteins or insertion of almost all kinds of membrane proteins: (1) Translation preceded by a loop insertion resulting in translocation across the membrane (e.g., secretory proteins), and (2) translation preceded by the channel insertion without loop resulting in accumulation in the cytosol (e.g., cytosolic domains of membrane proteins or signal anchor proteins). For polytopic membrane proteins, these two states would alternate. Thus, the sealing properties of the translocating channel and the

gap between the channel and the ribosome, as others and we observe it, would significantly reduce the regulatory and spatial requirements for the RNC-PCC complex in processes such as release of cytosolic domains and partitioning of transmembrane domains into the bilayer. Furthermore, seal-like behavior of the Sec61 complex may also maintain the permeability barrier of the membrane in posttranslational or retrograde protein translocation.

The spatial arrangement of the RNC-PCC complex containing nascent chains of polytopic integral membrane proteins or associated with additional translocon components will be addressed in future studies.

Experimental Procedures

Purification of Ribosome-Nascent Chain Complexes

For the generation of RNCs we used a cell-free yeast translation system, which was programmed with truncated synthetic mRNA coding for the 120 N-terminal amino acids of the type II membrane protein dipeptidylpeptidase B (DPAP-B). An additional N-terminal HA-tag (YPYDVPDYA) was used for the immunopurification of the stalled RNCs.

Capped mRNA was synthesized using the SP6 polymerase-based Message Machine kit from Ambion with DNA fragments as templates. The DNA fragments were generated by PCR, with the full-length gene as a template and extended primers. The 5′-primer added a SP6 site, followed by a high initiation efficiency 5′-untranslated region, an optimized AUG context and, in case of the tagged construct, the additional 9 amino acids of the HA-tag (5′-ATTTAGG TGACACTATAGAAACCAAACAAAACAAATAAAACAAAAACACAAT GTCTTACCCATACGATGTTCCAGATTACGCTGAAGGTGGCGAAGA AGAAGTTG-3′). The 3′-primer determined the length of the nascent chain (5′-ATCGTAGACAGATTTAACAACGTA-3′ for HA-DP-120). The amounts of mRNA in translation reactions were optimized for each batch of yeast extract.

The yeast translation extracts were prepared and used as previously described (Waters and Blobel, 1986). We used a haploid strain derived from DF5α. Gel filtration of the extract was carried out in buffer A (20 mM HEPES [pH 7.5], 100 mM KOAc, 2 mM Mg(OAc)$_2$, 2 mM DTT, 0.5 mM PMSF, and 10% w/v glycerol). The extract was treated with nuclease S7, frozen in liquid nitrogen, and stored at $-80°C$.

The 100 μl translation reaction contained 33% yeast extract ($\sim$100 OD$_{260}$/ml), 20 mM HEPES (pH 7.5), 150 mM KOAc, 2.5 mM Mg(OAc)$_2$, 2 mM DTT, 20 mM creatine phosphate, 0.1 mg/ml creatine kinase, 1 mM ATP, 0.5 mM GTP, 0.1 mg/ml yeast tRNA, 0.2 mM amino acids, 3.3% glycerol, 0.8 U/μl RNAsin (Promega), and ^{35}S-methionine (NEN). Reactions were incubated for 70 to 90 min at 17°C and terminated by addition of 2 μl of 10 mg/ml cycloheximide. Aliquots were analyzed by SDS-PAGE. After subsequent semidry blotting onto nitrocellulose membranes, proteins were visualized with amido black. The membranes were dried and exposed to X-ray film or probed with α-HA antibody followed by ECL detection (Amersham).

Analytical immunopurification of RNCs was performed by using a 100 μl reaction as starting material for each type of nascent chain. The purification was done as described below for the preparative purification except that the amounts of reagents and volumes were 5- to 8-fold smaller.

Preparative immunopurification was performed with 8 × 100 μl reactions. After addition of cycloheximide, two reactions were combined and spun through 800 μl of a high salt sucrose cushion (50 mM Tris.Cl [pH 7.0], 500 mM KOAc, 25 mM Mg(OAc)$_2$, 2 mM DTT, 1 M sucrose, 10 μg/ml cycloheximide, 0.1% Nikkol, and 0.1% pill/ml [1 pill complete protease mix/ml H$_2$O, Boehringer Mannheim]) at 355,000 g$_{av}$ for 45 min. Each of the resulting pellets was resuspended in 200 μl of ice-cold buffer B (32.5 mM Tris.Cl [pH 7.0], 125 mM KOAc, 26.25 mM Mg(OAc)$_2$, 1.5 mM DTT, 250 mM sucrose, 100 μg/ml cycloheximide, 0.1% Nikkol, 0.1% pill/ml, and 0.4 U/μl RNAsin). 4 μg of a biotinylated anti-HA antibody (clone 12CA5 from Boehringer Mannheim) was added, followed by incubation for 60 min on ice

and 30 min at RT. Each suspension was then added to 3 mg of equilibrated (2 × 200 µl buffer B) streptavidin-coupled magnetic beads (Dynabeads M-280 Strepavidin from Dynal) and incubated for 30 min at RT. The beads were washed with 2 × 400 µl of ice cold buffer B and 2 × 400 µl ice cold buffer C (50 mM Tris.Cl [pH 7.0], 500 mM KOAc, 25 mM Mg(OAc)$_2$, 1 mM DTT, 250 mM sucrose, 100 µg/ml cycloheximide, 0.1% Nikkol, 0.1% pill/ml, and 0.4 U/µl RNAsin). To elute the bound RNCs, the beads were incubated with 200 µl of buffer C including 1 mg/ml HA peptide (Boehringer Mannheim) for 30 min on ice and 15 min at RT. After rinsing of the beads with 100 µl buffer C, eluates were combined in two fractions of 600 µl and each spun through a 400 µl high salt sucrose cushion as described above. The resulting pellets were slowly resuspended in 50–100 µl of buffer G (20 mM Tris.Cl [pH 7.0], 50 mM KOAc, 10 mM Mg(OAc)$_2$, 1 mM DTT, 125 mM sucrose, 100 µg/ml cycloheximide, 0.05% Nikkol, 0.5% pill/ml, and 0.2 U/µl RNAsin), shock frozen, and stored at −80°C. The concentration of the final fraction was between 2.5 and 5 OD$_{260}$/ml corresponding to an overall yield of about 5–10 pmol. Aliquots of the various purification steps were precipitated with 7% trichloroacetic acid in the presence of deoxycholate for analysis by SDS-PAGE.

Reconstitution of RNC-Sec61 Complexes

The Sec61 complex was purified as previously described (Beckmann et al., 1997). Exchange of detergent from Triton X-100 to DeoxyBigChap (DBC, Calbiochem) was done essentially as described by Gorlich and Rapoport (1993) by binding of the complex to SP-Sepharose (Pharmacia) followed by equilibration and elution in 0.2% DBC. Before reconstitution with RNCs or empty ribosomes, the Sec61 complex in DBC and Triton X-100 was dialyzed at a molecular cutoff of 3.5 kDa against 20 mM Tris.Cl (pH 7.0), 100 mM KOAc, 5 mM Mg(OAc)$_2$, and 1 mM DTT.

RNC-Sec61 complexes were reconstituted by incubating 0.25 pmol of RNCs in a volume of 25 µl with 4–40 fold molar excess of Sec61 in 0.2% DBC or 1% Triton X-100. The incubation was done in the presence and absence of lipids (0.4 mg/ml of phosphatidyl-choline and phosphatidylethanolamine, 4:1) for 10 min on ice and 15 min at RT in 30 mM Tris.Cl (pH 7.0), 100 mM KOAc, 10 mM Mg(OAc)$_2$, 1.5 mM DTT, 12.5 mM sucrose, 8% glycerol, 20 µg/ml cycloheximide, and 0.005% Nikkol. Protease protection was assayed by subsequent addition of 2.7 µl of 0.1 mg/ml proteinase K solution and incubation on ice for 15 min. The reaction was stopped by addition of 2.5 µl 0.1 M PMSF, precipitated with trichloroacetic acid, and analyzed by SDS-PAGE followed by autoradiography.

For cryo-EM, 1 pmol RNCs was reconstituted with a 10-fold excess of DBC-Sec61 complex in a volume of 20 µl under the described conditions without lipids. Empty ribosome-Sec61 complexes were generated by a mock translation reaction in the absence of mRNA and the presence of 0.5 mM puromycin. The ribosomes were spun through a high salt sucrose cushion as described above, resuspended in buffer G, and reconstituted with the DBC-Sec61 complex for cryo-EM as described for RNCs.

Electron Microscopy and Image Processing

Cryo-EM grids were prepared as described (Wagenknecht et al., 1988). Micrographs were recorded in a defocus range between 1.7 µm and 6.0 µm on a Philips CM200 and a Philips F20 (FEI/Philips, Eindhoven) at a magnification of about 52,000× and scanned on a HiScan drum scanner (Eurocore, Saint-Denis) with a pixel size of 4.68 Å on the object scale.

The data were analyzed using the SPIDER system. After automated particle selection and visual verification, the data sets were subdivided into defocus groups and refined CTF-corrected 3D reconstructions were calculated as described (Gabashvili et al., 2000). The resolution was estimated by the Fourier shell correlation with a cutoff value of 0.5. The falloff of Fourier amplitudes toward higher spatial frequencies was corrected as described previously (Gabashvili et al., 2000), using the X-ray solution scattering intensity distribution of 70S ribosomes from *E. coli*.

For the translating complex, a subset of 22,788 particles in 30 defocus groups was used for the 3D reconstruction at a final resolution of 15.4 Å. In an attempt to estimate the occupancy of RNCs with channel, this dataset was sorted according to the presence of

density in the channel position, resulting in two subsets consisting of 17,934 (+channel) and 10,492 particles (−channel), which were used for independent reconstructions (not shown). For the non-translating complex, a subset of 18,519 particles in 23 defocus groups was used for the 3D reconstruction at a final resolution of 18.9 Å.

The data for the map shown in Figure 3b of the empty ribosome (purified as described (Beckmann et al., 1997) from the strain *Egd2aprA*) were collected on a Philips CM12, and a set of 14,028 particles in 10 defocus groups between 0.8 µm and 2.7 µm was used for the 3D reconstruction at a final resolution of 24.8 Å.

Separation of rRNA and protein density of the ribosomal subunits (Spahn et al., 2000), as well as calculation and docking of RNA and protein structure models, is described in the accompanying paper by Spahn et al., 2001. Visualization and interpretation of the maps and the docked models was done using SPIDER, IRIS Explorer (Numerical Algorithms Group, Inc., Downers Grove, IL), O (Jones et al., 1991), Ribbons (Carson, 1991), and POV-Ray.

References

Agrawal, R.K., Penczek, P., Grassucci, R.A., Li, Y., Leith, A., Nierhaus, K.H., and Frank, J. (1996). Direct visualization of A-, P-, and E-site transfer RNAs in the Escherichia coli ribosome. Science *271*, 1000–1002.

Agrawal, R.K., Spahn, C.M., Penczek, P., Grassucci, R.A., Nierhaus, K.H., and Frank, J. (2000). Visualization of tRNA movements on the Escherichia coli 70S ribosome during the elongation cycle. J. Cell Biol. *150*, 447–460.

Ban, N., Nissen, P., Hansen, J., Moore, P.B., and Steitz, T.A. (2000). The complete atomic structure of the large ribosomal subunit at 2.4 A Resolution. Science *289*, 905–920.

Beckmann, R., Bubeck, D., Grassucci, R., Penczek, P., Verschoor, A., Blobel, G., and Frank, J. (1997). Alignment of conduits for the nascent polypeptide chain in the ribosome-Sec61 complex. Science *278*, 2123–2126.

Bernabeu, C., Tobin, E.M., Fowler, A., Zabin, I., and Lake, J.A. (1983). Nascent polypeptide chains exit the ribosome in the same relative position in both eucaryotes and procaryotes. J. Cell Biol. *96*, 1471–1474.

Blobel, G., and Sabatini, D.D. (1970). Controlled proteolysis of nascent polypeptides in rat liver cell fractions. I. Location of the polypeptides within ribosomes. J. Cell Biol. *45*, 130–145.

Borel, A.C., and Simon, S.M. (1996). Biogenesis of polytopic membrane proteins: membrane segments assemble within translocation channels prior to membrane integration. Cell *85*, 379–389.

Carson, M. (1991). Ribbons 2.0. Appl. Cryst. *24*, 103–106.

Chuck, S.L., and Lingappa, V.R. (1992). Pause transfer: a topogenic sequence in apolipoprotein B mediates stopping and restarting of translocation. Cell *68*, 9–21.

Collinson, I., Breyton, C., Duong, F., Tziatzios, C., Schubert, D., Or, E., Rapoport, T., and Kuhlbrandt, W. (2001). Projection structure and oligomeric properties of a bacterial core protein translocase. EMBO J. *20*, 2462–2471.

Crowley, K.S., Liao, S., Worrell, V.E., Reinhart, G.D., and Johnson, A.E. (1994). Secretory proteins move through the endoplasmic reticulum membrane via an aqueous, gated pore. Cell *78*, 461–471.

Frank, J., Zhu, J., Penczek, P., Li, Y., Srivastava, S., Verschoor, A.,

Radermacher, M., Grassucci, R., Lata, R.K., and Agrawal, R.K. (1995). A model of protein synthesis based on cryo-electron microscopy of the E. coli ribosome. Nature 376, 441–444.

Gabashvili, I.S., Agrawal, R.K., Spahn, C.M., Grassucci, R.A., Svergun, D.I., Frank, J., and Penczek, P. (2000). Solution structure of the E. coli 70S ribosome at 11.5 Å resolution. Cell 100, 537–549.

Gabashvili, I.S., Gregory, S.T., Valle, M., Grassucci, R., Worbs, M., Wahl, M.C., Dahlberg, A.E., and Frank, J. (2001). Role of ribosomal proteins L4 and L22 in gating mechanisms of the polypeptide tunnel system. Mol. Cell 8, 181–188.

Gerbi, S.A. (1996). Expansion segment: regions of variable size that interrupt the universal core secondary structure of ribosomal RNA. In Ribosomal RNA: Structure, Evolution, Processing, and Function in Protein Synthesis. R.A. Zimmermann and A.E. Dahlberg, eds. (New York: CRC Press), pp. 71–87.

Gilmore, R., and Blobel, G. (1985). Translocation of secretory proteins across the microsomal membrane occurs through an environment accessible to aqueous perturbants. Cell 42, 497–505.

Gomez-Lorenzo, M.G., Spahn, C.M., Agrawal, R.K., Grassucci, R.A., Penczek, P., Chakraburtty, K., Ballesta, J.P., Lavandera, J.L., Garcia-Bustos, J.F., and Frank, J. (2000). Three-dimensional cryo-electron microscopy localization of EF2 in the Saccharomyces cerevisiae 80S ribosome at 17.5 Å resolution. EMBO J. 19, 2710–2718.

Görlich, D., and Rapoport, T.A. (1993). Protein translocation into proteoliposomes reconstituted from purified components of the endoplasmic reticulum membrane. Cell 75, 615–630.

Hamman, B.D., Chen, J.C., Johnson, E.E., and Johnson, A.E. (1997). The aqueous pore through the translocon has a diameter of 40–60 Å during cotranslational protein translocation at the ER membrane. Cell 89, 535–544.

Hamman, B.D., Hendershot, L.M., and Johnson, A.E. (1998). BiP maintains the permeability barrier of the ER membrane by sealing the lumenal end of the translocon pore before and early in translocation. Cell 92, 747–758.

Hanein, D., Matlack, K.E., Jungnickel, B., Plath, K., Kalies, K.U., Miller, K.R., Rapoport, T.A., and Akey, C.W. (1996). Oligomeric rings of the Sec61p complex induced by ligands required for protein translocation. Cell 87, 721–732.

Hegde, R.S., and Lingappa, V.R. (1996). Sequence-specific alteration of the ribosome-membrane junction exposes nascent secretory proteins to the cytosol. Cell 85, 217–228.

Heinrich, S.U., Mothes, W., Brunner, J., and Rapoport, T.A. (2000). The Sec61p complex mediates the integration of a membrane protein by allowing lipid partitioning of the transmembrane domain. Cell 102, 233–244.

Johnson, A.E., and van Waes, M.A. (1999). The translocon: a dynamic gateway at the ER membrane. Annu. Rev. Cell Dev. Biol. 15, 799–842.

Jones, T.A., Zhou, J.Y., Cowan, S.W., and Kjeldgaard, M. (1991). Improved methods for building protein models in electron density maps and the location of errors in these models. Acta Crystallogr. A A47, 110–119.

Jungnickel, B., and Rapoport, T.A. (1995). A posttargeting signal sequence recognition event in the endoplasmic reticulum membrane. Cell 82, 261–270.

Kalies, K.U., Gorlich, D., and Rapoport, T.A. (1994). Binding of ribosomes to the rough endoplasmic reticulum mediated by the Sec61p-complex. J. Cell Biol. 126, 925–934.

Keenan, R.J., Freymann, D.M., Stroud, R.M., and Walter, P. (2001). The Signal Recognition Particle. Annu. Rev. Biochem. 70, 755–775.

Liao, S., Lin, J., Do, H., and Johnson, A.E. (1997). Both lumenal and cytosolic gating of the aqueous ER translocon pore are regulated from inside the ribosome during membrane protein integration. Cell 90, 31–41.

Manting, E.H., van Der Does, C., Remigy, H., Engel, A., and Driessen, A.J. (2000). SecYEG assembles into a tetramer to form the active protein translocation channel. EMBO J. 19, 852–861.

Martoglio, B., Hofmann, M.W., Brunner, J., and Dobberstein, B. (1995). The protein-conducting channel in the membrane of the endoplasmic reticulum is open laterally toward the lipid bilayer. Cell 81, 207–214.

Matlack, K.E., Plath, K., Misselwitz, B., and Rapoport, T.A. (1997). Protein transport by purified yeast Sec complex and Kar2p without membranes. Science 277, 938–941.

Matlack, K.E., Mothes, W., and Rapoport, T.A. (1998). Protein translocation: tunnel vision. Cell 92, 381–390.

Ménétret, J., Neuhof, A., Morgan, D.G., Plath, K., Radermacher, M., Rapoport, T.A., and Akey, C.W. (2000). The structure of ribosome-channel complexes engaged in protein translocation. Mol. Cell 6, 1219–1232.

Meyer, T.H., Menetret, J.F., Breitling, R., Miller, K.R., Akey, C.W., and Rapoport, T.A. (1999). The bacterial SecY/E translocation complex forms channel-like structures similar to those of the eukaryotic Sec61p complex. J. Mol. Biol. 285, 1789–1800.

Morgan, D.G., Menetret, J.F., Radermacher, M., Neuhof, A., Akey, I.V., Rapoport, T.A., and Akey, C.W. (2000). A comparison of the yeast and rabbit 80 S ribosome reveals the topology of the nascent chain exit tunnel, inter-subunit bridges and mammalian rRNA expansion segments. J. Mol. Biol. 301, 301–321.

Mothes, W., Heinrich, S.U., Graf, R., Nilsson, I., von Heijne, G., Brunner, J., and Rapoport, T.A. (1997). Molecular mechanism of membrane protein integration into the endoplasmic reticulum. Cell 89, 523–533.

Mothes, W., Jungnickel, B., Brunner, J., and Rapoport, T.A. (1998). Signal sequence recognition in cotranslational translocation by protein components of the endoplasmic reticulum membrane. J. Cell Biol. 142, 355–364.

Ng, D.T., Brown, J.D., and Walter, P. (1996). Signal sequences specify the targeting route to the endoplasmic reticulum membrane. J. Cell Biol. 134, 269–278.

Nissen, P., Hansen, J., Ban, N., Moore, P.B., and Steitz, T.A. (2000). The structural basis of ribosome activity in peptide bond synthesis. Science 289, 920–930.

Palczewski, K., Kumasaka, T., Hori, T., Behnke, C.A., Motoshima, H., Fox, B.A., Le Trong, I., Teller, D.C., Okada, T., Stenkamp, R.E., et al. (2000). Crystal structure of rhodopsin: A G protein-coupled receptor. Science 289, 739–745.

Plath, K., Mothes, W., Wilkinson, B.M., Stirling, C.J., and Rapoport, T.A. (1998). Signal sequence recognition in posttranslational protein transport across the yeast ER membrane. Cell 94, 795–807.

Prinz, A., Behrens, C., Rapoport, T.A., Hartmann, E., and Kalies, K.U. (2000). Evolutionarily conserved binding of ribosomes to the translocation channel via the large ribosomal RNA. EMBO J. 19, 1900–1906.

Shaw, A.S., Rottier, P.J., and Rose, J.K. (1988). Evidence for the loop model of signal-sequence insertion into the endoplasmic reticulum. Proc. Natl. Acad. Sci. USA 85, 7592–7596.

Simon, S.M., and Blobel, G. (1991). A protein-conducting channel in the endoplasmic reticulum. Cell 65, 371–380.

Spahn, C.M., Penczek, P.A., Leith, A., and Frank, J. (2000). A method for differentiating proteins from nucleic acids in intermediate-resolution density maps: cryo-electron microscopy defines the quaternary structure of the Escherichia coli 70S ribosome. Struct. Fold. Des. 8, 937–948.

Spahn, C.M., Beckmann, R., Eswar, N., Penczek, P.A., Sali, A., Blobel, G., and Frank, J. (2001). Structure of the 80S ribosome from Sacharomyces cerevisiae—tRNA-ribosome and subunit-subunit interactions. Cell 107, this issue, 373–386.

Stark, H., Orlova, E.V., Rinke-Appel, J., Junke, N., Mueller, F., Rodnina, M., Wintermeyer, W., Brimacombe, R., and van Heel, M. (1997). Arrangement of tRNAs in pre- and posttranslational ribosomes revealed by electron cryomicroscopy. Cell 88, 19–28.

Sweeney, R., Chen, L., and Yao, M.C. (1994). An rRNA variable region has an evolutionarily conserved essential role despite sequence divergence. Mol. Cell. Biol. 14, 4203–4215.

Unwin, P.N., and Zampighi, G. (1980). Structure of the junction between communicating cells. Nature 283, 545–549.

Wagenknecht, T., Grassucci, R., and Frank, J. (1988). Electron mi-

croscopy and computer image averaging of ice-embedded large ribosomal subunits from Escherichia coli. J. Mol. Biol. *199*, 137–147.

Wang, L., and Dobberstein, B. (1999). Oligomeric complexes involved in translocation of proteins across the membrane of the endoplasmic reticulum. FEBS Lett. *457*, 316–322.

Waters, M.G., and Blobel, G. (1986). Secretory protein translocation in a yeast cell-free system can occur posttranslationally and requires ATP hydrolysis. J. Cell Biol. *102*, 1543–1550.

Wilkinson, B.M., Critchley, A.J., and Stirling, C.J. (1996). Determination of the transmembrane topology of yeast Sec61p, an essential component of the endoplasmic reticulum translocation complex. J. Biol. Chem. *271*, 25590–25597.